width is 30 – 50 μm. A dependence of the intensity of generation on the target length has been examined experimentally. Saturation of lasing has been achieved, and a reliable estimate of the small-signal effective gain (~ 30 cm^{-1}) has been obtained; the maximum energy of laser X-ray radiation does not exceed approximately 1 μJ.

References

1. Lindl J *Phys. Plasmas* **2** 3933 (1995)
2. Andre M L, in *IFSA 99 — Inertial Fusion Sciences and Applications* (The Data Science Library, Vol. 2, Eds C Labaune, W J Hogan, K A Tanaka) (Amsterdam: Elsevier, 2000) p. 32
3. Kirillov G A et al. *Laser Part. Beams* **18** 219 (2000)
4. Perry M D et al. *Opt. Lett.* **24** 160 (1999)
5. Norreys P A, Krushelnick K M, Zepf M *Plasma Phys. Control. Fusion* **46** B13 (2004)
6. Tanaka K A et al. *Plasma Phys. Control. Fusion* **46** B41 (2004)
7. Gadzhieva V V et al. *Voprosy At. Nauki Tekh. Ser. Mat. Mod. Fiz. Prots.* (3) 25 (2000)
8. Karlykhanov N G et al. *Pis'ma Zh. Eksp. Teor. Fiz.* **79** 30 (2004) [*JETP Lett.* **79** 25 (2004)]
9. Wilson D C, Krauser W J, in *Laser Interaction with Matter: Proc. of the 23rd European Conf.* (Inst. of Phys. Conf. Ser., No. 140, Ed. S J Rose) (Bristol: IOP Publ., 1995) p. 459
10. Zuev A I *Zh. Vychisl. Mat. Mat. Fiz.* **32** 82 (1992) [*Comput. Math. Math. Phys.* **32** 70 (1992)]; Barysheva N M et al. *Zh. Vychisl. Mat. Mat. Fiz.* **22** 401 (1982) [*Comput. Math. Math. Phys.* **22** 156 (1982)]
11. Shushlebin A N et al., in *Vychislitel'nye Tekhnologii* (Computational Techniques) Vol. 4, No. 13 (Novosibirsk: Institut Vychislitel'nykh Tekhnologii SO RAN, 1995) p. 336
12. Chizhkov M N et al. *Laser Part. Beams* **23** 261 (2005)
13. Amendt P et al. *Phys. Plasmas* **9** 2221 (2002)
14. Nikiforov A F, Uvarov V B *Dokl. Akad. Nauk SSSR* **191** 47 (1970) [*Sov. Phys. Dokl.* **15** 191 (1970)]
15. Nikiforov A F, Novikov V G, Uvarov V B *Kvantovo-statisticheskie Modeli Vysokotemperaturnoi Plazmy: Metody Rascheta Rosselandovykh Probegov i Uravnenii Sostoyaniya* (Quantum-Statistical Models of High-Temperature Plasma: Computing Methods for Rosseland Lengths and Equations of State) (Moscow: Fizmatlit, 2000) [Translated into English: *Quantum-Statistical Models of Hot Dense Matter: Method for Computation and Equation of State* (Basel: Birkhäuser Verlag, 2005)]
16. Andriyash A V, Simonenko V A *Fiz. Plazmy* **14** 1201 (1988) [*Sov. J. Plasma Phys.* **14** 703 (1988)]
17. Stein J, Shalitin D, Ron A *Phys. Rev. A* **31** 446 (1985)
18. Cox A N, Stewart J N, Eilers D D *Astrophys. J. Suppl. Ser.* **11** 1 (1965)
19. Carson T R, Mayers D F, Stibbs D W N *Mon. Not. R. Astron. Soc.* **140** 483 (1968)
20. Dyall K G et al. *Comput. Phys. Commun.* **55** 425 (1989)
21. Parpia F A, Fischer C F, Grant I P *Comput. Phys. Commun.* **94** 249 (1996)
22. Loboda P A et al., in *Proc. XXVIII European Conf. on Laser Interaction with Matter: ECLIM, Rome, Italy, 6 – 10 September 2004*, p. 383; SPECTR-W^3, http://spectr-w3.snz.ru
23. WIS List of Databases for Atomic and Plasma Physics, http://plasma-gate.weizmann.ac.il/DBfAPP.html
24. Loboda P A et al. *Laser Part. Beams* **18** 275 (2000)
25. Magunov A I et al. *Pis'ma Zh. Eksp. Teor. Fiz.* **74** 412 (2001) [*JETP Lett.* **74** 375 (2001)]
26. Loboda P A et al. *J. Phys. A: Math. Gen.* **39** 4781 (2006)
27. Bar-Shalom A et al. *Phys. Rev. A* **40** 3183 (1989)
28. Bar-Shalom A, Oreg J, Goldstein W H *Phys. Rev. E* **51** 4882 (1995)
29. Cowan R D *The Theory of Atomic Structure and Spectra* (Berkeley: Univ. of California Press, 1981)
30. Springer P T et al. *Phys. Rev. Lett.* **69** 3735 (1992)
31. Dmitrov D A et al., in *Proc. XXVIII European Conf. on Laser Interaction with Matter: ECLIM, Rome, Italy, 6 – 10 September 2004*, p. 591
32. Wharton K B et al. *Phys. Rev. Lett.* **81** 822 (1998)
33. Potapov A V et al., in *Tezisy 11-i Vseross. Konf. po Diagnostike Vysokotemperaturnoi Plazmy* (Digest of 11th All-Russia Conf. on High-Temperature Plasma Diagnostics), *Troitsk, Moscow region, June 13 – 18, 2005* (Moscow: RNTs 'Kurchatovskii Institut', 2005)
34. Politov V Yu, Lykov V A, Shinkarev M K *Proc. SPIE* **1928** 157 (1993)
35. Politov V Yu, Potapov A V, Antonova L V *Laser Part. Beams* **18** 291 (2000)
36. Andriyash A V et al. *Fiz. Plazmy* **32** 156 (2006) [*Plasma Phys. Rep.* **32** 135 (2006)]
37. Andriyash A V et al. "Izuchenie generatsii neitronov v T(d, n)^{4}He i D(d, n)^{3}He reaktsiyakh na 10 TW pikosekundnoi lazernoi ustanovke Sokol-P" ("Study of neutron production in T(d, n)^{4}He and D(d, n)^{3}He reactions using the 10-TeV picosecond Sokol-P laser facility"), in *VIII Zababakhinskie Nauchnye Chteniya* (8th Zababakhin Scientific Readings), *Snezhinsk, 2005*; http://www.vniitf.ru/rig/konfer/8zst/plenar/plen.htm
38. Bychenkov B Yu, Tikhonchuk V T, Tolokonnikov S V *Zh. Eksp. Teor. Fiz.* **115** 2080 (1999) [*JETP* **88** 1137 (1999)]
39. Andriyash A V et al. *Kvantovaya Elektron.* **36** 511 (2006) [*Quantum Electron.* **36** 511 (2006)]

PACS numbers: 05.10.Ln, 05.70.Jk, 75.40.Cx
DOI: 10.1070/PU2006v049n10ABEH006099

Monte Carlo studies of critical phenomena in spin lattice systems

A K Murtazaev

1. Introduction

The basic ideas of modern phase transition and critical phenomena theories are those associated with and involved in the scaling and universality hypotheses and renormalization group theory [1, 2].

Although it was believed until very recently that static phase transitions and critical phenomena have been fully explored and do not really need anything more in terms of theory, now the study of frustrated systems, magnetic superlattices, and spin systems with quenched nonmagnetic disorder shows that this is by far not the case [2 – 4].

Applied to such systems, traditional theoretical and experimental methods run into serious difficulties in an attempt to calculate critical parameters and to uncover the nature and peculiarities of critical behavior (including the mechanisms behind them), which led to the intense use of Monte Carlo (MC) methods in studies of phase transitions and critical phenomena in these systems [3 – 5].

The subject matter of this report is the critical behavior of the 3D Ising model with quenched nonmagnetic order for the example of cubic lattice and that of a model that was suggested to describe a real iron – vanadium superlattice $[Fe_2/V_{13}]_L$.

There are quite a number of reasons for interest in the critical behavior of such systems and their models. An actively discussed topic in the field has been that of how quenched nonmagnetic disorder affects the critical properties of spin lattice systems [2 – 4, 6 – 8]. In an important step, the so-called Harris criterion was developed within the framework of renormalized perturbation theory, which predicts, on a qualitative level, when and whether a particular impurity is of great concern in determining critical behavior [9]. According to this criterion, nonmagnetic disorder does play a role only in the situation when the specific heat critical exponent is positive, $\alpha > 0$: a condition which is satisfied only if the

effective Hamiltonian of the system is isomorphic to the Ising model near the critical point.

While it is a well-established fact, theoretically, numerically, and experimentally, that nonmagnetic impurities change the critical exponents of the Ising model [2–4, 7], the question remains if the new critical exponents of a given model are universal — that is, independent of the impurity concentration up to the percolation threshold — or whether a certain line of fixed points exists which determines the continuous variation of these critical exponents with the concentration. In addition, there is every reason to believe that critical parameters depend on exactly how disorder was introduced into the model at hand [6].

Given, further, the inconsistent nature of the available experimental data [10, 11], a no less interesting and hardly less confusing situation exists with regard to the critical properties of magnetic sublattices. While the values of some critical exponents correspond to 2D systems, those of others are characteristic of 3D systems. The fact that Fe/V superlattices display the critical exponents expected for 3D systems points to the importance of interlayer interaction for describing critical behavior. Exposing a superlattice to a hydrogen atmosphere causes hydrogen to penetrate into the vanadium sublattice and so to change the thickness of the vanadium intervening layer, thus allowing one to continuously change the nature of this interaction from antiferromagnetic to ferromagnetic. Because the amount of absorbed hydrogen depends on pressure, it follows that at a certain external pressure the interlayer interaction can be reduced to zero — with the result that transitions from 3D magnetism to 2D magnetism and back again can be observed. Because critical exponents are highly sensitive parameters, their calculation will make it possible to sufficiently accurately determine the universality classes of the critical behavior of such systems, as well as the peculiarities and conditions of the transition (crossover) from 3D to 2D magnetism.

2. Ising model with quenched disorder, and the investigation technique

2.1 Ising model with quenched disorder

The Ising model with quenched disorder is outlined in Fig. 1. If the impurity distribution in our model is assumed to be canonical, then:

(1) the sites of the cubic lattice carry spins S_i that take the following values $S_i = \pm 1$ and contain nonmagnetic impurities (vacancies) that are distributed randomly and fixed;

(2) the binding energy between two sites is zero if at least one site is occupied by a nonmagnetic atom, and equals $|J|$ if both are occupied by magnetic atoms.

The microscopic Hamiltonian of such a system can be written down as

$$H = -\frac{J}{2}\sum_{i,j} \rho_i S_i \rho_j S_j \,, \tag{1}$$

where

$$\rho_i = \begin{cases} 1\,, & \text{if the site carries a spin}\,, \\ 0\,, & \text{if the site is occupied by a nonmagnetic impurity.} \end{cases}$$

The concentration p of magnetic spins is determined by summing the absolute value of the spin over all lattice sites,

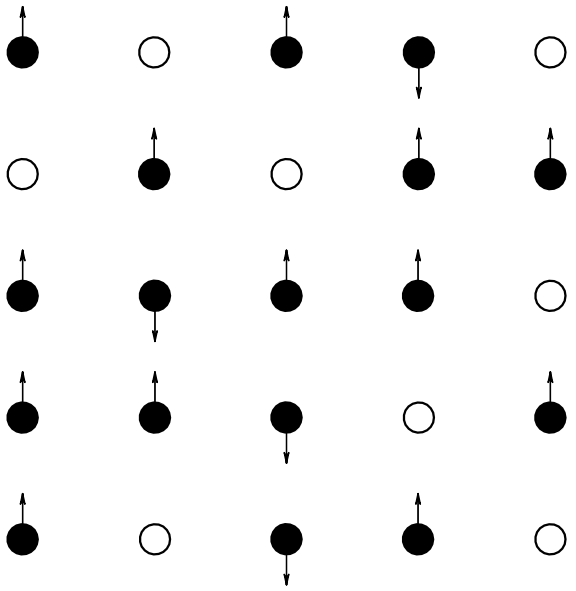

Figure 1. A weakly diluted Ising model with quenched nonmagnetic impurities.

namely

$$p = \frac{1}{L^3}\sum_{i=1}^{L^3} \rho_i |S_i| \,. \tag{2}$$

The values $p = 1$ and $p = 0$ correspond to the pure Ising model and an empty impurity-only lattice, respectively.

2.2 Investigation technique

Cluster MC algorithms have proven to be a powerful, reliable, and highly efficient tool for studying critical phenomena in various systems and models [12] (see also references cited in the papers [4, 5, 8]). Our choice among these was the Wolff algorithm, currently viewed to be the most efficient. Its specific realization in our study is as follows.

(1) A lattice site is selected randomly. If the site is found to harbor a nonmagnetic impurity, another lattice site is selected randomly, and so on until a site with a magnetic spin S_i has been encountered.

(2) All the nearest neighbors S_j of a given spin S_i are examined. If a neighboring site is occupied by a magnetic spin, then, with the probability $p = 1 - \exp(-2K)$ (where $K = J/k_B T$, k_B is the Boltzmann constant, and T is the temperature), a link is established between S_j and S_i, provided S_j and S_i have equal values for $J > 0$. This is followed by scanning the nearest neighbors of the last spin with which a link was established. This process continues until the boundaries of the system are reached.

(3) All those spins having links established between themselves form a 'cluster'.

(4) The cluster so obtained flips with the probability unity.

Calculations were performed for systems with periodic boundary conditions and linear dimensions $L \times L \times L = N$, $L = 20-60$, at spin concentrations $p = 1.0, 0.95, 0.9, 0.8, 0.7, 0.65$, and 0.60. Initial configurations were specified in such a way that all the spins were aligned along the z-axis. To bring a system into the thermodynamically equilibrium state, nonequilibrium regions of length up to 6×10^6 MC steps per spin were cut off (here, one MC step per spin corresponds to one

flip of a cluster), and an averaging over 50 to 80 various initial configurations was carried out.

It should be remembered that simultaneously with decreasing magnetic site concentration, the impurity distribution over the lattice fluctuates stronger, requiring that more impurity configurations with various disorder realizations be used for averaging various thermodynamic parameters. Notice that modeling large-sized lattices takes much more computational effort for each impurity configuration.

2.3 Results

To see how specific heat and susceptibility of the system progressed with temperature we resorted to the fluctuation relations (see references cited in the papers [4, 5])

$$C = (NK^2)\left(\langle U^2\rangle - \langle U\rangle^2\right), \tag{3}$$

$$\chi = (NK)\left(\langle m^2\rangle - \langle m\rangle^2\right), \tag{4}$$

where $K = J/k_{\mathrm{B}}T$, $N = pL^3$ is the number of magnetic sites, U is the internal energy, m is the system's magnetization, and angle brackets denote ensemble averaging. The critical temperature was determined using the fourth-order Binder cumulant U_L [4–7]:

$$U_L(T,P) = 1 - \frac{\langle m^4(T,p;L)\rangle}{3\langle m^2(T,p;L)\rangle^2}, \tag{5}$$

where m is the magnetization of a system possessing the linear dimension L. In this method, the critical temperature T_{c} is determined as the point where the temperature dependences of the cumulants U_L constructed for systems of various linear dimensions L intersect.

Figure 2 depicts the characteristic temperature dependences of specific heat C for systems with different spin concentrations. It should be noted that as the concentration of nonmagnetic impurities $c = 1 - p$ increases, the specific heat and susceptibility peaks (in analogous dependences) shift toward lower temperatures and get lower and higher, respectively. Figure 3 shows the characteristic temperature dependence of averaged Binder cumulants $U_L(T,p)$ for systems with different linear dimensions at the spin concentration $p = 0.65$. The point of intersection of these curves corresponds to the critical temperature.

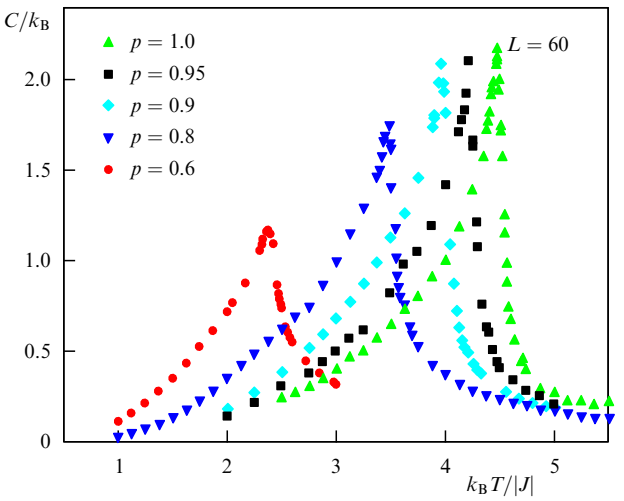

Figure 2. Specific heat versus temperature for a 3D Ising model with nonmagnetic impurities ($L = 60$).

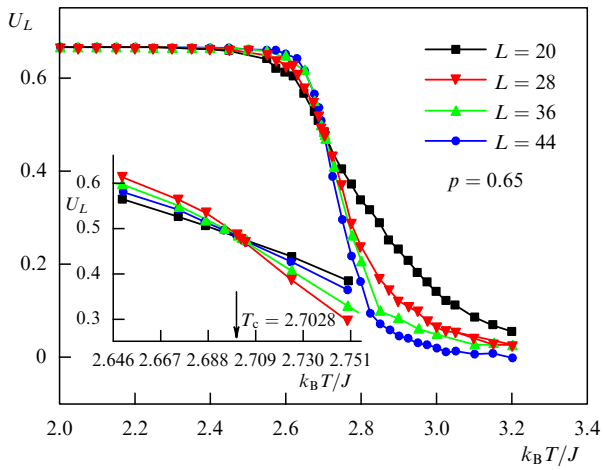

Figure 3. Binder cumulants U_L averaged over impurity configurations, as functions of temperature for a system with $p = 0.65$.

The specific heat, susceptibility, magnetization, and correlation radius critical exponents (denoted by α, γ, β, and ν, respectively) were determined by employing finite-size scaling theory in which, for sufficiently large systems with periodic boundary conditions, the near-T_{c} behavior of the basic thermodynamic functions — the free energy F, specific heat C, susceptibility χ, and magnetization m — scales in the following way [13]:

$$F(T,L) \sim L^{-d}F_0(tL^{1/\nu}), \tag{6}$$

$$C(T,L) \sim L^{\alpha/\nu}C_0(tL^{1/\nu}), \tag{7}$$

$$\chi(T,L) \sim L^{\gamma/\nu}\chi_0(tL^{1/\nu}), \tag{8}$$

$$m(T,L) \sim L^{-\beta/\nu}m_0(tL^{1/\nu}), \tag{9}$$

where $t = |T - T_{\mathrm{c}}|/T_{\mathrm{c}}$, with $T_{\mathrm{c}} = T_{\mathrm{c}}(L = \infty)$, and α, β, γ, ν are the statistical critical exponents for which the hyperscaling relationship $2 - \alpha = \mathrm{d}\nu = 2\beta + \gamma$ holds true [1].

Furthermore, finite-size scaling theory can be used to determine ν, the critical exponent of the correlation radius. This is done by noting that

$$V_n = L^{1/\nu}g_{V_n}, \tag{10}$$

where g_{V_n} is a certain constant, and the role of V_n can be played by

$$V_n = \frac{\langle m^n U\rangle}{\langle m^n\rangle} - \langle U\rangle, \qquad n = 1,2,3,4. \tag{11}$$

From relationships (8), (9) it follows that at $T = T_{\mathrm{c}}$, the susceptibility and magnetization obey the following relations:

$$\chi \sim L^{\gamma/\nu}, \tag{12}$$

$$m \sim L^{-\beta/\nu}. \tag{13}$$

It is these relations which we used in evaluating γ and β. To approximate the temperature dependence of specific heat on L, in practice other expressions are normally applied, for example, the following ones [4, 5]:

$$C_{\max}(L) = C_{\max}(L = \infty) - AL^{\alpha/\nu}, \tag{14}$$

where A is a certain factor.

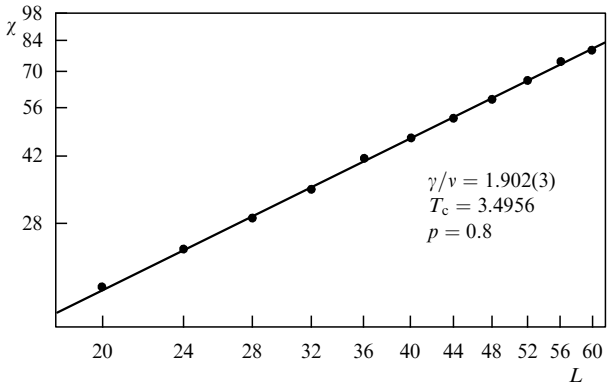

Figure 4. Log-log plot of susceptibility χ versus linear dimension L for a system with $p = 0.8$.

The critical exponents α, β, γ, and ν were calculated by constructing the L-dependences of C, m, χ, and V_n. The nonlinear least square analysis of the data yielded the values of α/ν, β/ν, γ/ν, $1/\nu$, and then the values of ν obtained in the framework of this study were utilized for determining the critical exponents α, β, γ.

Figure 4 falls back on a log-log scale to represent the characteristic dependence of the susceptibility on the linear lattice dimension L for the spin concentration $p = 0.8$. It should be emphasized that the susceptibility data obtained in this study do not deviate from a straight line even at small values of L. Clearly, the number of impurity configurations we used for averaging and the dimensions $L \geqslant 20$ of the systems studied did enable the asymptotic critical regime to be reached. These conditions were secured for all the other systems studied as well. Importantly, we calculated the exponent ν directly from numerical simulation results obtained in the framework of the study, whereas many others leant upon various types of scaling relations for the purpose.

In Table 1 are shown the values of critical exponents for different values of p, as calculated for a corresponding $\nu(p)$. It can be seen that the critical exponents in the covered range of concentrations p differ from the corresponding values for a pure system. As regards the slight concentration dependence displayed by the critical exponents of a weakly diluted system ($p \geqslant 0.8$), the crossover from the pure system to a diluted one could be the explanation.

Table 1. Finite-size scaling results for the critical exponents of a 3D Ising model with quenched nonmagnetic impurities.

p	$k_B T_c/\lvert J\rvert$	ν	α	γ	β
1.0	4.5106(6)	0.624(2)	0.108(2)	1.236(2)	0.322(2)
0.95	4.2591(4)	0.646(2)	−0.010(2)	1.262(2)	0.306(3)
0.9	4.0079(8)	0.664(3)	−0.014(3)	1.285(3)	0.308(3)
0.8	3.4956(6)	0.683(4)	−0.016(3)	1.299(3)	0.310(3)
0.7	2.9682(8)	0.716(6)	−0.087(6)	1.431(6)	0.341(6)
0.65	2.7028(9)	0.708(8)	−0.091(8)	1.426(8)	0.343(8)
0.6	2.4173(9)	0.725(9)	−0.093(9)	1.446(9)	0.349(9)

At strong dilutions ($p < 0.7$), the corresponding exponents are seen to increase markedly in absolute values — possibly due to the presence of another random fixed point which, if it exists, is necessarily characterized by a new set of critical exponents. This scenario of a critical behavior seems indeed to be the case according to the experimental work reported in Ref. [14], where the critical exponents for diluted $Fe_pZn_{1-p}F_2$ magnetics with $p = 0.6$ and $p = 0.5$ are found to be practically identical to what we obtained for $p = 0.6$.

The type of critical behavior we saw occur at strong dilution ($p < 0.7$) is consistent with the assumed influence of another — 'percolation' — fixed point [15, 16]. Also note, finally, that for $p = 1.0$ our values of critical exponents are in excellent agreement with those currently considered standard [3–5].

3. $[Fe_2/V_{13}]_L$ superlattice model and the investigation technique

3.1 $[Fe_2/V_{13}]_L$ superlattice model

$[Fe_2/V_{13}]_L$ superlattices are the most interesting ones in which to study critical properties and, possibly, the crossover from 3D to 2D magnetism. It should be noted that, with the iron layer only two monolayers thick, every iron atom in these superlattices possesses four nearest neighbors in the adjacent iron layer. The iron layers are shifted with respect to each other by a half lattice constant along the x- and y-axes. The interaction between the nearest neighbors is ferromagnetic in nature and determined by the intralayer exchange parameter $J_\parallel$. In addition to that, the atoms of iron layers interact with each other through the vanadium layers (interlayer interaction), the coupling parameter $J_\perp$ depending both for its magnitude and sign on the iron layer separation, i.e., on the hydrogen atmosphere pressure [10, 11]. The magnetic moments of the iron atoms are aligned in the xy-plane. A schematic of a vanadium–iron superlattice is given in Fig. 5. The Hamiltonian of such a system can be represented in the form of a modified three-dimensional xy-model, namely

$$H = -\frac{1}{2}\sum_{i,j} J_\parallel (S_i^x S_j^x + S_i^y S_j^y) - \frac{1}{2}\sum_{i,k} J_\perp (S_i^x S_k^x + S_i^y S_k^y)\,, \tag{15}$$

where the first (second) sum accounts for the exchange interaction between a magnetic atom and the nearest neighbors within the layer (between a magnetic atom and one atom in the neighboring layer, through the vanadium intervening layer), while S_i^x and S_i^y are the spin projections on the x- and y-axes. The interlayer-to-intralayer exchange ratio $J_\perp/J_\parallel$ depends on the iron layer separation which in turn depends on how much hydrogen the vanadium layers have adsorbed. In our model $r = J_\perp/J_\parallel$ is a specified parameter and can be varied from $r = -1.0$ to $r = 1.0$.

3.2 Investigation technique

The calculations were performed on model systems with periodic boundary conditions and linear dimensions

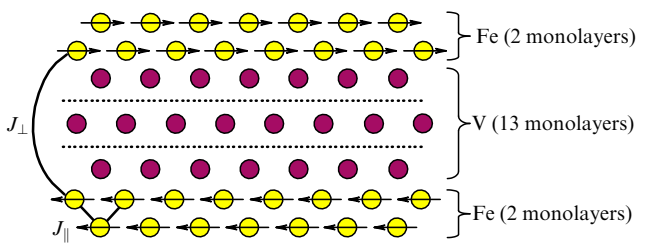

Figure 5. Schematic of a vanadium–iron superlattice $[Fe_2/V_{13}]_L$.

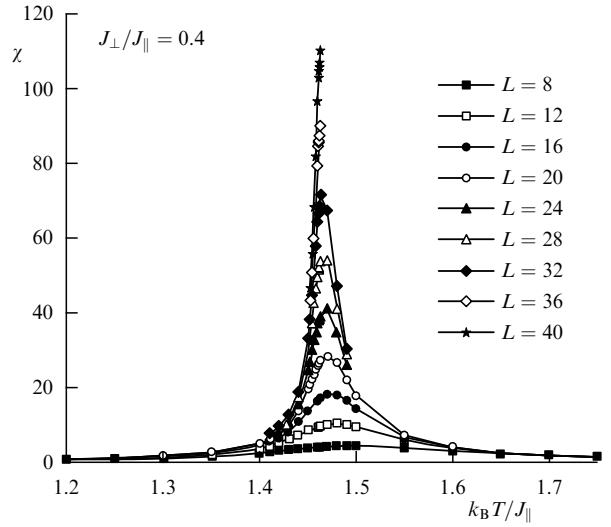

Figure 6. Temperature dependence of susceptibility for a model of a magnetic superlattice $[Fe_2/V_{13}]_L$ at $r = J_\perp/J_\parallel = 0.4$.

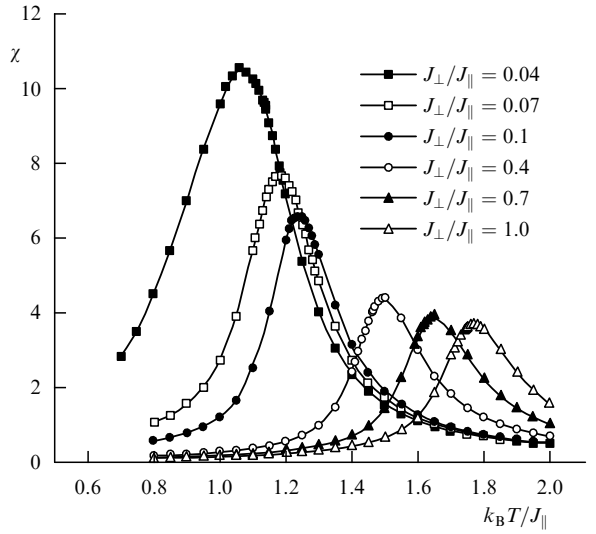

Figure 7. Susceptibility versus temperature for various values of $r = J_\perp/J_\parallel$.

Table 2. Critical exponents for the model of magnetic superlattice Fe_2/V_{13}.

$J_\perp/J_\parallel$	$k_B T_c/J_\parallel$	ν_{av}	α	β	γ	$\alpha + 2\beta + \gamma$
1.0	1.7463(3)	0.6706(3)	−0.0184(3)	0.3417(3)	1.3398(3)	2.0048
0.7	1.6197	0.6696	−0.0099	0.3392	1.3284	1.9969
0.4	1.4616	0.6689	−0.0068	0.3380	1.3289	1.9981
0.1	1.2219	0.6617	0.0187	0.3284	1.3231	1.9986
0.07	1.1832	0.6618	0.0288	0.3267	1.3243	2.0065
0.04	1.1346	0.6548	0.0635	0.3166	1.3172	2.0139
0.01	1.0559	0.6012	0.1621	0.2878	1.2298	1.9675

$L \times L \times L = N$ ($L = 8-40$ is the number of magnetic Fe layers) using the same Wolff single-cluster algorithm (a version of the MC method) described in Section 2.2. To bring a system into the thermodynamically equilibrium state, a nonequilibrium region of the Markov chain with length up to 3×10^4 MC steps per spin was cut off. Thermodynamic variables were averaged along a Markov chain of length up to 1.2×10^6 Monte Carlo steps per spin. Initial configurations were specified in such a way that all the spins were aligned along the x-axis.

3.3 Results

Thermodynamic parameters and critical exponents were calculated using the methodology similar to that described in Section 2.3.

To keep watch on the peculiarities of behavior of the specific heat and susceptibility, relationships (3) and (4) were applied. A typical temperature dependence of the susceptibility χ for systems of various sizes but with the same interlayer-to-intralayer exchange ratio $r = 0.4$ is displayed in Fig. 6. We see that as the linear dimensions of the system increase, the susceptibility peak $\chi_{max}(L)$ rises and shifts toward lower temperatures. The specific heat shows similar behavior, but in this case the peaks $C_{max}(L)$ shift to higher temperatures. The value of T_c was determined using the method of Binder cumulants. The fourth-order Binder cumulants U_L were calculated from formula (5) and then, similarly to Fig. 3, temperature dependences of U_L were constructed for various values of L. As follow from the analysis of critical temperatures obtained for various values of r, the critical temperature decreases with decreasing r, consistent with the results of laboratory measurements [17]. Shown in Fig. 7 are typical susceptibility-vs-temperature curves for various values of interlayer-to-intralayer exchange ratio r. Similar dependences were also obtained for the specific heat. As r decreases, the specific heat and susceptibility peaks shift towards lower temperatures, their heights decreasing and increasing, respectively.

The critical exponents α of the specific heat, γ of the susceptibility, and β of the magnetization and the correlation radius were calculated using the methodology and analytical expressions described in Section 2.3. Table 2 lists the values of all critical parameters calculated for various values of r. Notice that at $r = 1.0$, our model corresponds to the classical xy-model. The critical exponents we determined for this case agree to high accuracy with the best values found by other methods for the xy-model [1, 5].

Decreasing the parameter r results in a smooth change in the values of the critical exponents, and up to a certain threshold the critical exponents obey the well-known scaling relations (for example, the Rushbrook relation) [1]. However, at $r = 0.01$, the critical exponents undergo a significant change in their values and at the same time the scaling relations between them break down, all this presumably marking the transition from 3D to 2D magnetism at the above-indicated boundary value of r. It should be emphasized that the temperature dependences of some thermodynamic parameters also show at $r = 0.01$ some characteristic features absent at larger values of r, suggesting that $r = 0.01$ can be viewed as a threshold value and that for $r < 0.01$ the system can be considered quasi-two-dimensional.

4. Conclusions

Presented in this report is a study, within a unified research framework, of the critical properties of a 3D diluted Ising model with canonically distributed nonmagnetic impurities and of a modified xy-model supposed to describe the peculiarities of iron–vanadium superlattices (Fe/V).

(1) Our data indicate that at low impurity concentrations ($p \geqslant 0.8$), the nonmagnetically-doped Ising model forms a new universality class different from that of the pure Ising model ($p = 1.0$).

(2) Strongly diluted systems ($p \leqslant 0.7$) are characterized by a different set of critical exponents and form a universality class of their own.

In this case there are also two crossover regions:

(1) between a pure system ($p = 1.0$) and weakly diluted ($p \geqslant 0.8$) systems, and

(2) between weakly diluted ($p \approx 0.8$) and strongly diluted ($p \leqslant 0.7$) systems.

Possibly, it is the existence of the crossover and the large extent of these regions which explains the inconsistent and sometimes conflicting results the study of this model has produced.

The results obtained with the modified xy-model provide insight into how and when a magnetic superlattice makes a transition from the three-dimensional behavior to the quasi-two-dimensional. The critical exponents show dependence on the ratio of the interlayer-to-intralayer exchange interaction. At the same time, the values of the critical exponents obey scaling relations for values of r up to a threshold value of $r = 0.01$.

The author wishes to thank I K Kamilov, K Sh Khizriev, A B Babaev, V M Uzdin, and Yu B Kudasov for their interest to my work, a steady help and fruitful discussions during the course of the work.

The work was done under financial support from the Russian Foundation for Basic Research (grant No. 04-02-16487) and the National Science Assistance Fund.

References

1. Patashinskii A Z, Pokrovskii V L *Fluktuatsionnaya Teoriya Fazovykh Perekhodov* (Fluctuation Theory of Phase Transitions) 2nd ed. (Moscow: Nauka, 1982) [Translated into English — 1st Russian edition (Oxford: Pergamon Press, 1979)]
2. Dotsenko V S *Usp. Fiz. Nauk* **165** 481 (1995) [*Phys. Usp.* **38** 457 (1995)]
3. Folk R, Holovatch Yu, Yavors'kii T *Usp. Fiz. Nauk* **173** 175 (2003) [*Phys. Usp.* **46** 169 (2003)]
4. Murtazaev A K, Kamilov I K, Babaev A B *Zh. Eksp. Teor. Fiz.* **126** 1377 (2004) [*JETP* **99** 1201 (2004)]
5. Kamilov I K, Murtazaev A K, Aliev Kh K *Usp. Fiz. Nauk* **169** 773 (1999) [*Phys. Usp.* **42** 689 (1999)]
6. Wiseman S, Domany E *Phys. Rev. E* **58** 2938 (1998)
7. Ballesteros H G et al. *Phys. Rev. B* **58** 2740 (1998)
8. Vasilyev O A, Shchur L N *Zh. Eksp. Teor. Fiz.* **117** 1110 (2000) [*JETP* **90** 964 (2000)]
9. Harris A B *J. Phys. C: Solid State Phys.* **7** 1671 (1974)
10. Rüdt C et al. *Phys. Rev. B* **65** 220404 (2002)
11. Pärnaste M et al. *Phys. Rev. B* **71** 104426 (2005)
12. Wolff U *Phys. Rev. Lett.* **62** 361 (1989)
13. Fisher M E, Barber M N *Phys. Rev. Lett.* **28** 1516 (1972)
14. Birgeneau R J et al. *Phys. Rev. B* **27** 6747 (1983)
15. Prudnikov V V, Vakilov A N *Zh. Eksp. Teor. Fiz.* **103** 962 (1993) [*JETP* **76** 469 (1993)]
16. Heuer H-O *J. Phys. A: Math. Gen.* **26** L333 (1993)
17. Leiner V et al. *Phys. Rev. Lett.* **91** 37202 (2003)

PACS numbers: 78.70.Gq, 84.40.Fe, 84.47.+w
DOI: 10.1070/PU2006v049n10ABEH006109

Relativistic multiwave oscillators and their possible applications

V A Cherepenin

This report is a brief review of advances in a rapidly developing realm of science — relativistic high-frequency electronics. The term relativistic high-frequency electronics is presently used in reference to that area of vacuum electronics which harnesses electron beams with energies of 0.2–100 MeV and currents up to 10^4 A. The resultant microwave oscillators (MOs) range up to 10^9-10^{10} W in power for a pulse duration of $10^{-9}-10^{-7}$ s. The wavelengths utilized in this field lie in the interval from several dozen centimeters to values belonging to the visible range, i.e., span six orders of magnitude. Naturally, the family of the devices employed in these ranges is highly diversified. However, it turns out that many of them are well known in conventional microwave electronics. In this connection, of interest is the advancement of new ideas of vacuum electronics, aimed at raising the generated- or amplified-signal power and at mastering new wavelength ranges. The present report is concerned with this aspect of relativistic high-frequency electronics. It is pertinent to note that there are excellent reviews dedicated to relativistic high-frequency electronics and its application (see, for instance, Ref. [1]). Here, we endeavor to call attention to those aspects of the development of this area, which for several reasons have not been adequately discussed in the foregoing and other reviews.

The first vacuum devices — grid electron tubes — date back to the beginning of the 20th century and, having undergone a series of modifications, are employed to the present day. The shortest-wavelength devices can operate in the decimetric wavelength range. The output power of these devices can be quite high and some of their other characteristics, for instance, radiation resistance, give promise that they will, despite the rapid development of semiconductor devices, also find use in the future, at least in special-purpose tasks. The physical principles of the operation of grid electron tubes are well known even from school textbooks and do not call for analysis. We only mention the relatively recent ideas of employing them to produce high-power radiation by incorporating a great number of these devices into a transmission line. Broadly speaking, methods for making a high-power device out of many lower-power devices are vigorously being developed and sometimes come to fruition. Naturally, the last mentioned remark pertains to devices of any kind.

The 1920s–1940s saw the advent of microwave devices of a new type, in which the 'intrinsic' properties of the electron beam had profound significance: the time of electron transit through the interaction region, electron bunching, the space charge, etc. The electrodynamic notions of the quasistationary theory, like the induced current theorem or coupled transmission lines, were sufficient for their description and design. It was then that the vacuum devices which still enjoy wide use were invented and fabricated. It will suffice to mention klystrons, traveling-wave tubes (TWTs), backward-wave tubes (BWTs), and magnetrons.

Initially, work in the area of microwave electronics, as a rule, was unrelated to the self-radiation of charged particles (usually, electrons), which was viewed from the application